



Effect of low frequency, high power pool ultrasonics on viscosity of fluid food: Modeling and experimental validation



Monica Anese^a, Maria Valeria De Bonis^b, Giorgio Mirolo^a, Gianpaolo Ruocco^{b,*}

^a Dipartimento di Scienze degli Alimenti, Università degli Studi di Udine, Via Sondrio 2/a, Udine 33100, Italy

^b CFDFood, Scuola d'Ingegneria, Università degli Studi della Basilicata, Campus Macchia Romana, Potenza 85100, Italy

ARTICLE INFO

Article history:

Received 19 January 2013

Received in revised form 22 May 2013

Accepted 17 June 2013

Available online 2 July 2013

Keywords:

Ultrasonics

Viscosity

Non-newtonian

Natural convection

Tomato puree

Computational fluid dynamics

ABSTRACT

Ultrasound induced changes of certain physical and chemical properties of molecules are nowadays exploited at industrial level for food processing and preservation purposes. Deeper knowledge on the mechanisms influencing these changes would contribute to extend implementations of ultrasound to steer structure and functionality of food molecules.

In this study the laws of transfer phenomena were applied in order to investigate on the viscosity changes of a pectin-containing fluid flow, i.e. tomato puree in a cylindrical reactor, induced by low frequency, high intensity ultrasound treatments. In particular, the model for fluid motion was associated to a validating rheological investigation.

Results showed a good agreement between experimental and computational data for temperature and viscosity progresses with time. A new power law for viscosity has been proposed based on reactor aspect ratio and Rayleigh numbers for natural convection.

© 2013 Elsevier Ltd. All rights reserved.

1. Introduction

Food viscosity is an important processing and formulation parameter, as it may affect some unit operations, such as piping and mixing, as well as the rheological properties of the final product. As well known, viscosity is influenced by physical and chemical properties of polymers naturally contained in the food matrix (e.g. molecular weight, nature and number of functional groups, their position in the molecule).

Preliminary results have shown that ultrasounds (US), that are already applied for food processing and preservation (e.g. emulsification, homogenization, extraction, freezing, etc.), can induce changes in the physical properties (e.g. viscosity, water binding capacity, etc.) of biopolymers such as pectin, starch and proteins (McClements, 1995), to obtain ingredients or semi-manufactured products with tailored functional characteristics. Such effects are due to the cavitation phenomenon, which is the spontaneous formation and collapse of bubbles, that leads to the generation of local extreme temperatures and pressures, that in turn produce intense shear energy waves and turbulence in the vicinity of the material (Mason, 1998; Barbosa-Canóvas and Rodríguez, 2002).

The structural modifications of biopolymers are reported to highly depend on the US intensity and material nature (Vercet

et al., 2002a; Tiwari et al., 2010). In particular, power US may cause opposite effects on macromolecules. For instance, pectin, starch or protein containing systems that were exposed to high values of power showed a viscosity decrease due to depolymerization (Seshadri et al., 2003; Jambrak et al., 2009; Zuo et al., 2009). On the contrary, a viscosity increase (fluid thickening) was observed in food matrices such as tomato puree and yoghurt (Vercet et al., 2002a,b; Wu et al., 2008; Anese et al., 2013). It has been speculated that reducing the polymer size would liberate macromolecules and subsequently more polymer chain would be available for bonding (Seshadri et al., 2003). As a consequence US treatment can give rise to a different type of network, which is accompanied by an enhancement of the rheological properties.

The aim of the present paper was to study the interdependence of low frequency, high power US induced viscosity changes and flow field during treatment of a pectin-based fluid food, such as tomato puree. Most of the world's tomato crop is processed into tomato derivatives, such as tomato juice, paste, concentrate and powder (Gould, 1991). Tomato products are sold as convenient food in pre-packed packages or used as ingredients for the manufacture of a wide range of formulated foods.

In exploring the erratic nature of pool US or sonication, it is important to know the active bubbles generation and stronger cavitation patterns (Gogate et al., 2002), but the application of transfer phenomena laws is the key to macromolecular physical properties determination. In particular, process modeling by the Computational Fluid Dynamics (CFD) of the subject Non-Newtonian fluid

* Corresponding author. Tel.: +39 0971 205454; fax: +39 0971 205461.

E-mail address: gianpaolo.ruocco@unibas.it (G. Ruocco).

Nomenclature

c_p	specific heat (J/kg K)
g	gravitational acceleration (m/s ²)
H	vessel height (mm)
k	thermal conductivity (W/m K)
m	consistency index (Pa s ^{n})
n	power law index
p	pressure (Pa)
\dot{Q}	nominal acoustic power (W)
\dot{q}	power density (kW/m ³)
R	universal gas constant (kJ/mol K)
Ra	Rayleigh number
t	time (s)
T	temperature (°C)
\mathbf{u}	velocity vector (m/s)

Greek

α	thermal diffusivity (m ² /s)
β	thermal expansion coefficient (1/K)
$\dot{\gamma}$	shear rate (1/s)
η	dynamic viscosity (Pa s)
ρ	density (kg/m ³)
τ	shear stress (Pa)

Subscripts

0	initial, apparent
d	deep geometry
s	shallow geometry
∞	operating parameter

may be useful in assessing the process efficiency and helping establish the optimal configuration parameters.

Lei et al. (2006) introduced an acoustic streaming formulation in determining fluid motion by numerical techniques, including the buoyancy force due to horn heating. Their results focussed on flow fields and heat transfer, but no effects on rheology are reported. This limitation is also found in Laborde et al. (2000), where fluid dynamics phenomena and cavitation induced by power US have been studied, only. A wave equation formulation was then exploited by Klíma et al. (2007), but the flow patterns and their effects on fluid behavior were left unexplored. A similar approach was tried by Kumaresan et al. (2007), who complemented the computational aeroacoustics method with a number of turbulence paradigms. Their work confirmed the highly non-uniform nature of the situation at stake, but did not dig into the fluid alterations. In Xu et al. (2013), the flow field generated by a transducer at frequency of 490 kHz is simulated, by using a finite elements commercial solver. The model solves the harmonic wave field, following the inhomogeneous Helmholtz equation, to describe the acoustic pressure distribution. This is a complete approach to describe the flow field induced by the acoustic pressure, but the structural change of the liquid sample is neglected.

In this work, the physico-chemical thread leading from power US-induced kinetics changes and structure degradation to tomato puree thickening (structure and functionality) is substituted with a fluid dynamics, classical approach. A momentum and heat transfer model is proposed and solved by a commercial finite elements code, incorporating custom notations for rheology. Upon the inherent volumetric heating, a free convection pattern is established which alters the Non-Newtonian shear rate. Through experimental validation and model optimization, the model is able to simulate the local and mean histories of viscosity, velocity and temperature; a modified power law notation for apparent viscosity is then proposed, depending on US intensity and vessel geometry, shedding light on potential use of CFD to simulate complex rheological US-dependent configurations.

2. Experimental set-up and measurements

2.1. Sample preparation and treatment

Commercial tomato puree rates of 450 g (7.3 ± 0.8% dry matter), previously sieved to remove seeds and coarse particles, were poured into two different glass vessels. A schematic representation of the US reactor is shown in Fig. 1. In particular, one geometry had

$R = 75$ mm and $H = 70$ mm (hereafter called shallow geometry, s), another had $R = 50$ mm and $H = 120$ mm (deep geometry, d).

An ultrasonic processor (Hieschler Ultrasonics GmbH, mod. UP400S, Teltow, Germany) with a titanium horn tip with diameter of 22 mm was used (Fig. 1). Treatments were performed for 15 min at US amplitude and frequency of 100 μ m and 24 kHz, respectively. The horn was placed in the centre of the vessel, with an immersion depth in the fluid varying between 10 and 20 mm. In order to minimize water evaporation and promote thermal insulation during sonication, the vessel was closed with a Plexiglas lid fitted with holes allowing horn and thermocouple probes to be placed at the desired positions in the tomato puree. The nominal acoustic power was $\dot{Q} = 400$ W, bringing forth two different power densities: $\dot{q}_d = 425$ kW/m³ or $\dot{q}_s = 324$ kW/m³.

Sample temperature was kept at 60 °C during the treatment, by means of a thermostatic bath. The temperature history was recorded using copper-constantan thermocouple probes (Ellab, Denmark) connected to a data logger (CHY 502A1, Tersid, Milano, Italy). In particular, the temperature was measured in three fixed points of the sample mass, sufficiently far one another.

Upon treatment, at fixed times the samples were cooled down to 20 °C in an ice bath. After gentle mixing for thermal homogeneity, 50 g of tomato puree were sampled, immediately assayed for rheological measurements, and disposed of after assessment.

An adequate number of samples were taken as controls, by heating them at 60 °C in the same configuration, with no exposure to US. Both heat and US treatments were carried out in duplicate. By comparing the different treatments it was concluded that

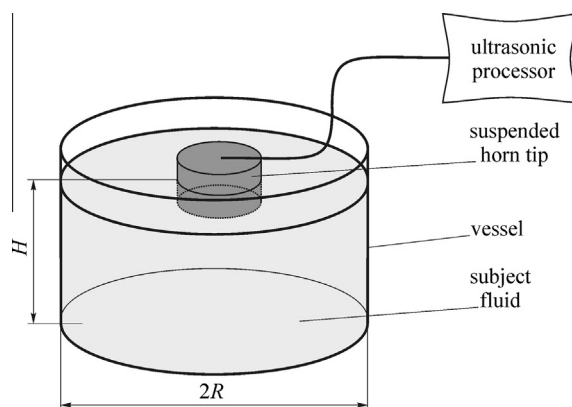


Fig. 1. Schematic representation of the ultrasonic reactor.

simple preheating in the bath gives reversible and negligible viscosity increments, while sonication results in an irreversible fluid thickening.

2.2. Rheological and total solids content measurements and analysis

Rheological determinations were performed at 20 °C constant temperature according to the method described by Vercet et al. (2002a). In particular, a Stresstech Rheometer (ReoLogica Instruments AB, Lund, Sweden) equipped with a concentric cylinder geometry (C25) was used. Viscosity was measured at a set shear rate, $\dot{\gamma}$, of 48.2 1/s, and both delay time and integration time at 5 s. $\dot{\gamma}$ was attained from the rheograms previously obtained for $\dot{\gamma}$ between 0.12 and 136 1/s. The rheogram of untreated tomato puree at ambient condition, showing a pseudoplastic behavior with yield stress, is provided in Fig. 2. Similar curves were obtained for the samples subjected to ultrasound treatments.

Total solids content was determined gravimetrically by drying the samples in a vacuum oven (1.32 kPa) at 75 °C at constant weight.

Chemical as well as rheological analyses were carried out at least five times on two replicated runs. One-way analysis of variance was carried out and differences among means were assessed by using the Tukey test (Statistica, Statsoft Inc., Cary, NC). Means were considered significantly different at $P < 0.05$.

3. Model formulation

3.1. Process description

In order to study the effect of power US on tomato puree viscosity a transient, 2D axial-symmetric model is implemented, corresponding to experimental capacities and sizes, to describe the inherent distributions of fluid motion (yielding strong local shear rate) and thickening as well as temperature (Fig. 3).

A number of assumptions are considered, to come up with a pseudo-kinetics effect to structural fluid changes.

3.2. Assumptions

1. Exposure to power US corresponds to an all-inclusive heat source term, \dot{q} in the energy equation.
2. Due to this volumetric heating, a free convection flow pattern is determined, which alters the shear rate.
3. The fluid is incompressible, in laminar flow, with constant properties except for the Non-Newtonian viscosity, η . The viscous heat dissipation is neglected.

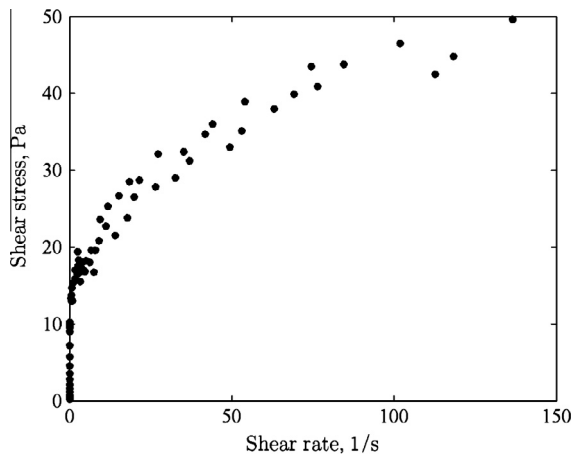


Fig. 2. Rheogram of an untreated tomato puree sample.

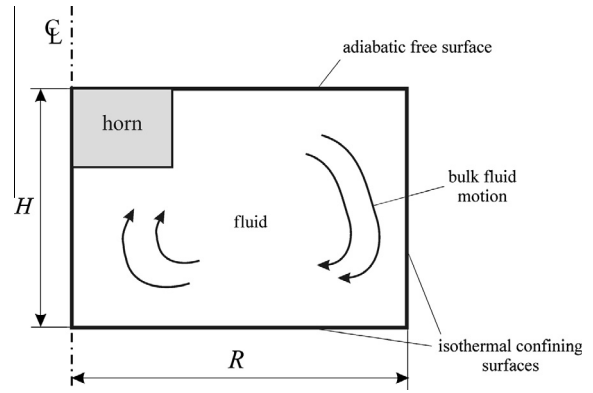


Fig. 3. Schematic representation of the 2D axial-symmetry geometry.

3.3. Governing equations

The governing conservation equations in vector form are enforced to yield for interdependent momentum and heat transfer (Bird et al., 2002):

Continuity:

$$\frac{\partial \rho}{\partial t} + \nabla \cdot (\rho \mathbf{u}) = 0 \quad (1)$$

Momentum:

$$\rho \left(\frac{\partial \mathbf{u}}{\partial t} + \mathbf{u} \cdot \nabla \mathbf{u} \right) = -\nabla p + \eta(\dot{\gamma}) \nabla^2 \mathbf{u} + \rho \mathbf{g} \beta (T - T_{\infty}) \quad (2)$$

The Non-Newtonian viscosity included here, $\eta(\dot{\gamma})$ (Bird et al., 2002), though function of shear rate (or local derivative of velocity vector, \mathbf{u}), will be the subject of special scrutiny later in the paper.

Energy:

$$\rho c_p \frac{\partial T}{\partial t} + \nabla \cdot (-k \nabla T) = -\rho c_p \mathbf{u} \cdot \nabla T + \dot{q} \quad (3)$$

3.4. Initial and boundary conditions

The fluid is initially at a uniform temperature $T_{\infty} = 60$ °C, with a initial viscosity at $\eta_0 = 0.18$ Pa s. Cooling through the free surface is negligible (it was evaluated as 5 order of magnitude smaller than the operating heat generation). With reference to Fig. 3, the following boundary conditions are adopted:

- slip condition with thermal insulation at the free surface, and symmetric conditions at centre line:

$$\mathbf{n} \cdot \mathbf{u} = 0; \quad \mathbf{n} \cdot \nabla T = 0 \quad (4)$$

- no-slip condition with imposed operating temperature, at bottom and lateral surfaces:

$$\mathbf{u} = 0; \quad T = T_{\infty} \quad (5)$$

3.5. Discretization of domains and run durations

A given computational grid for every geometry is adopted, by using Lagrange-quadratic elements. Several grids were tried, from a total of 300 triangular elements up to more than 1000. The final grid, yielding for grid-independency results, had some 500 triangular elements, and more than 6000 degrees of freedom.

A finite element commercial code has been employed to solve the system of partial differential equations (Multiphysics User's Guide, 2008). The GMRES solver is used for the algebraic system,

while the BDF method is adopted for time stepping. The run was executed for a total period of 15 min, taking less than a minute on a Supermicro PC carrying a Xeon CPU, under Windows XP.

4. Results and discussion

4.1. Measured viscosity progress

The effect of moisture changes on viscosity were almost negligible, as water loss during US treatment was always less than 1%. Control samples heated at 60 °C had viscosity very similar ($P > 0.005$) to that of unprocessed puree.

Measured values for viscosity are reported in Fig. 4, for both d and s geometries and two horn depths. The degree of fluid thickening depends first on the power density employed, as expected. Then it is noted that the progress is affected by a some fluctuation for the deep geometry, due to the inherent buoyancy on-set. An erratic behavior is detected when a deeper horn position is employed, for the fluid thickening progress is inverted at 600 s. At the end, it is evinced that the fluid thickening is unaffected by the horn depth, probably due to this high power intensity employed.

As anticipated earlier, the high US volumetric perturbation induces strong buoyancy patterns. The local fluid motion and pattern size depend on power density and reactor aspect ratio. It is speculated here that 2 different process spans exist (Fig. 4):

1. An initial ramp, especially evident for the d geometry.
2. A later period, in which the fluid in the s geometry keeps on thickening.

Therefore, fluid heating and shearing are strongly intertwined. In this paper a special relationship is proposed to describe this phenomenon.

4.2. A new viscosity correlation

Let us start with reporting on the inherent heat transfer. The process at stake is a complex one in that an internal heat generation and a fixed temperature boundary condition are present, at the same time. For free convection flows, buoyancy and viscous forces interplay, together with momentum and thermal diffusivities. The Rayleigh number is the dimensionless group that is usually invoked in such situations; for Non-Newtonian fluid, an

analytical treatment based on the Rayleigh number has been recently suggested by Vinogradov et al. (2011). In the present case, two different Rayleigh number notations should be considered, based on reactor height (Rohsenow et al., 1998):

$$Ra_q = \frac{\rho g \beta H^3 \dot{q} H^2}{\eta_0 \alpha 2k} \quad (6)$$

$$Ra_T = \frac{\rho g \beta H^3 (T - T_\infty)}{\eta_0 \alpha} \quad (7)$$

Note here the reference value of η employed. Now, while Ra_q is fixed and uniform during the process, given the power density and geometry, Ra_T changes with continuity and throughout the reactor volume during the treatment, distorting the fluid motion and, in turn, viscosity.

Based on these considerations, it is clear that a new viscosity notation would account for both the traditional shear rate concept ($\dot{\gamma}$, as determined by the local derivative of \mathbf{u} , as earlier already implied), and the special inherent heat transfer described above. Therefore, a generalized power law (after Herschel and Bulkley, Holdsworth (1993)) is first invoked, to ensure wide fluid applicability:

$$\eta = \eta_0 + m \dot{\gamma}^n \quad (8)$$

with m the consistency index (depending on the particular fluid at stake), and n the power law index.

By returning our attention again on Fig. 4, it is recalled that different phases of thickening increment or steadiness depend on the relative equilibrium between the two free convection mechanisms expressed by Ra_q and Ra_T . Therefore Eq. (8) is appropriately modified as follows:

$$\eta = \eta_0 + n_1 \frac{Ra_T}{Ra_q} + m \dot{\gamma}^n \quad (9)$$

4.3. Simulated mean viscosity and temperature progress

The model has been then preliminary run to evaluate its consistency, with respect to the experimental measurements, and reported in Fig. 5. All of thermophysical properties, other than viscosity, have been taken from Rao et al. (1981).

Phases 1 and 2 speculated earlier can be recognized, together with typical spikes due to abrupt distortion of fluid motion due to buoyancy and confinement. The comparisons hold nicely enough, when the following positions are adopted in Eq. (9): $m = 0.3$, $n = n_1 = R/H$. This way, the geometry aspect ratio is

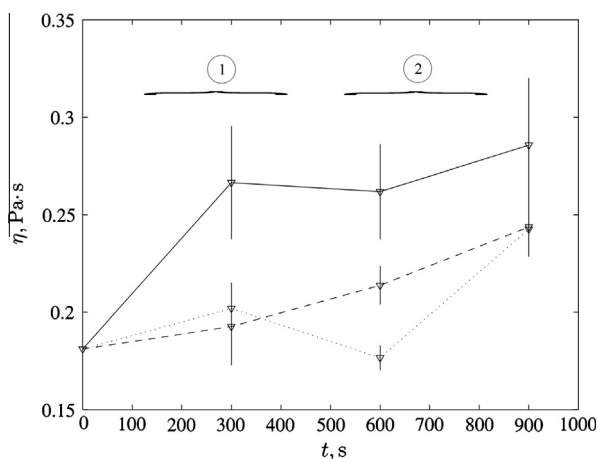


Fig. 4. Apparent viscosities, with related error bars, for 3 experimental runs: d geometry, with 10 mm horn depth (—); s geometry, with 10 mm horn depth (---); s geometry, with 20 mm horn depth (···).

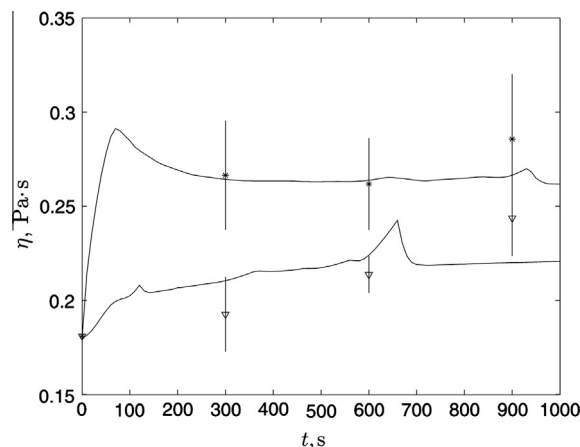


Fig. 5. Comparison of simulated mean viscosity (—) and experimental viscosity (with related error bars), for both d (*) and s (v) geometries.

adequately taken into account. A final notation for Non-Newtonian viscosity is therefore adopted:

$$\eta = \eta_0 + \frac{R}{H} \frac{Ra_T}{Ra_q} + m \dot{\gamma}^{R/H} \quad (10)$$

which restricts the number of parameters to be used and is in accord with the envisaged physical mechanisms.

In Fig. 6 is then presented the progress of simulated and experimental mean temperatures. For case d, the computation slightly overestimates the temperature by about 10% after 280 s, but at the end the two histories compare nicely. The temperature reaches 90 °C and 87 °C with \dot{q}_d or \dot{q}_s , respectively.

4.4. Viscosity distributions

The tool offered by the CFD allows one to locally inspect the distributions of viscosity, velocity and temperature during the treatment, evidencing the local distortion of the fluid, under the volumetric heating. Local viscosity, with maps of velocity and temperature are reported in Figs. 7 and 8, respectively. The fluid is

readily affected by thickening, right after 100 s (Fig. 7, left), due to the downdraft motion at the reactor wall (for its colder temperature). As the boundary layer develops (after 500 s, in Fig. 7, center), its relatively small thickness favors the fluid distortion and consequent shear rate increment. The fluid pattern is already established at mid process duration; at the end (after 1000 s, in Fig. 7, right), a slight increase of minimum viscosity is detected only, with its location still floating laterally to the wall, while no increase of maximum viscosity is found, its location still identified at mid-height, adjacent to the vertical wall. It is seen therefore that the fluid thickening process is already completed after just 500 s, in the considered reactor and for the power density employed, due to the onset of the flow pattern at stake.

Finally, it is also useful to inspect the temperature maps in Fig. 8. The indication of local viscosity are again reported. It is clear that after 1000 s of treatment, under the intense volumetric heating, a heated fluid build-up is found at the free top surface. This is due to the natural convection regime which makes the warm fluid to float upward, with a downward stream by the lateral wall (as earlier speculated) which cannot achieve complete thermal homogeneity. This indication is useful to evaluate inherent consequences

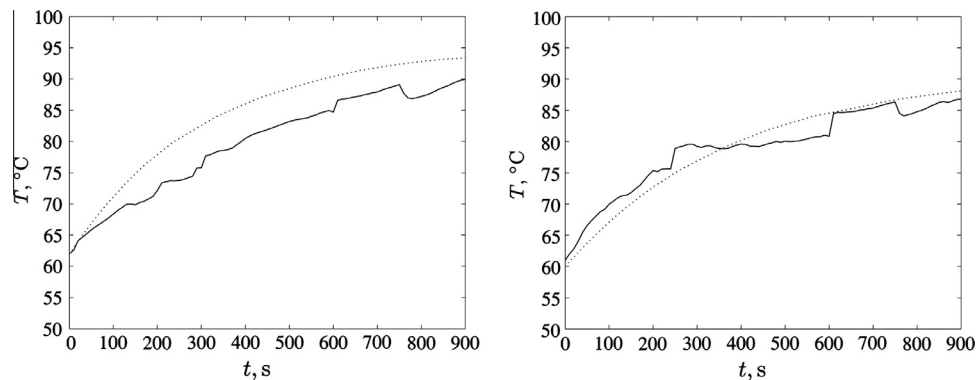


Fig. 6. Comparison of simulated (···) mean and experimental (—) mean temperatures, for both d (left) and s (right) geometries.

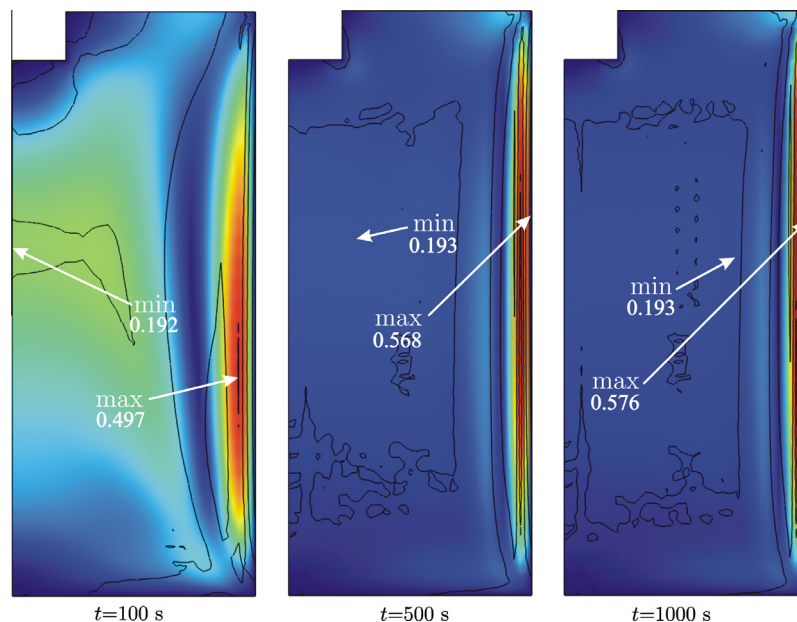


Fig. 7. Maps of velocity for the d geometry, at 100, 500 and 1000 s times, in the 0–0.0021 m/s range, with underlying distribution of viscosity (Pa s), with indication of minimum and maximum loci.

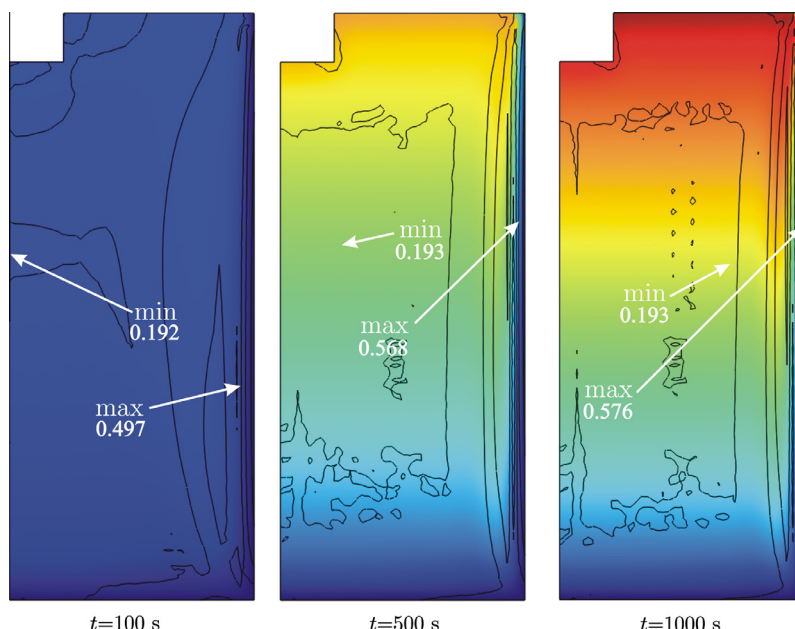


Fig. 8. Maps of temperature for the d geometry, at 100, 500 and 1000 s times, in the range 335–395 K range, with underlying distribution of viscosity (Pa s), with indication of minimum and maximum loci.

of thermal run-away, that may deteriorate some fluid functional property of interest.

5. Conclusions

Computational fluid dynamics was used to predict viscosity distribution in a Non-Newtonian, macromolecule containing fluid, such as tomato pulp, subjected to low frequency, high intensity ultrasound treatments in vessels with different geometries. An equation for viscosity changes based on Rayleigh numbers was formulated, that takes into account the vessel geometry. Model validation was performed based on data from rheological investigation. Results agree well with actual observations. Fluid thickness mainly increased in the first steps of ultrasonic processing due to the flow field induced by volumetric heating. The extent of fluid thickening was dependant on vessel geometry, being more pronounced in the deeper reactor. The general principle employed here allows for implementations with different geometries and power intensities, within the enforced assumptions. This would allow one to steer ultrasound process to obtain products with tailored functional properties.

Acknowledgement

MA conceived the study and carried out the experiments in conjunction with GM. MVDB and GR developed the model. MVDB carried out the computations and set up the model validation. All Authors participated in manuscript revisions and discussion, coordinated and critiqued by GR.

References

- Anese, M., Mirolo, G., Beraldo, P., Lippe, G., 2013. Effect of ultrasound treatments on microstructure and lycopene in vitro bioaccessibility of tomato pulp. *Food Chemistry* 136, 458–463.
- Barbosa-Canóvas, G.V., Rodríguez, J.J., 2002. Update on non-thermal food processing technologies: pulsed electric field, high hydrostatic pressure, irradiation and ultrasound. *Food Australia* 54, 513–518.
- Bird, R.B., Stewart, W.E., Lightfoot, E.N., 2002. *Transport Phenomena*. John Wiley & Sons, New York.
- Gogate, P.R., Tatake, P.A., Kanthale, P.M., Pandit, A.B., 2002. Mapping of sonochemical reactors: review, analysis, and experimental verification. *AIChE Journal* 48, 1542–1560.

- Gould, W.A., 1991. *Tomato Production, .. Processing & Technology*, Third ed. CTI Publications Inc., Timonium, ML.
- Holdsworth, S.D., 1993. Rheological models used for the prediction of the flow properties of food products. A literature review. *Transactions of the Institution of Chemical Engineering* 71, 139–179.
- Jambrak, A.R., Lelas, V., Mason, T.J., Krešić, G., Badanjak, M., 2009. Physical properties of ultrasound treated soy proteins. *Journal of Food Engineering* 93, 386–393.
- Klíma, J., Frias-Ferrer, A., Gonzáles-García, J., Ludvík, J., Sáez, V., Iniesta, J., 2007. Optimisation of 20 kHz sonoreactor geometry on the basis of numerical simulation of local ultrasonic intensity and qualitative comparison with experimental results. *Ultrasonics Sonochemistry* 14, 19–28.
- Kumaresan, T., Kumar, A., Pandit, A.B., Joshi, J.B., 2007. Modeling flow pattern induced by ultrasound: the influence of modeling approach and turbulence models. *Industrial & Engineering Chemistry Research* 46, 2936–2950.
- Laborde, J.L., Hita, A., Caltagirone, J.P., Gerard, A., 2000. Fluid dynamics phenomena induced by power ultrasounds. *Ultrasonics* 38, 297–300.
- Lei, H., Henry, D., BenHadid, H., 2006. Numerical study of the influence of a longitudinal sound field on natural convection in a cavity. *International Heat and Mass Transfer* 49, 3601–3616.
- Mason, T.J., 1998. Power ultrasound in food processing – the way forward. In: Povey, M.J.W., Mason, T.J. (Eds.), *Ultrasound in Food Processing*. Blackie Academic and Professional, London, pp. 105–126.
- McClements, J.D., 1995. Advances in the application of ultrasound in food analysis and processing. *Trends in Food Science & Technology* 6, 293–299.
- COMSOL Multiphysics User's Guide, COMSOL AB., 2008.
- Rao, M.A., Bourne, M.C., Cooley, H.J., 1981. Flow properties of tomato concentrates. *Journal of Texture Studies* 12, 521–583.
- Rohsenow, W.M., Hartnett, J.P., Cho, Y.I., 1998. *Handbook of Heat Transfer*, third ed. McGraw-Hill, New York (US).
- Seshadri, R., Weiss, J., Hulbert, G.J., Mount, J., 2003. Ultrasonic processing influences rheological and optical properties of high-methoxyl pectin dispersions. *Food Hydrocolloids* 17, 191–197.
- Tiwari, B.K., Muthukumarappan, K., O'Donnell, C.P., Cullen, P.J., 2010. Rheological properties of sonicated guar, xanthan and pectin dispersions. *International Journal of Food Properties* 13, 223–233.
- Vercet, A., Sánchez, C., Burgos, J., Montanes, L., López-Buesa, P., 2002a. The effects of manothermosonication on tomato pectin enzymes and tomato paste rheological properties. *Journal of Food Engineering* 53, 273–278.
- Vercet, A., Oria, R., Marquina, P., Crelier, S., López-Buesa, P., 2002b. Rheological properties of yoghurt made with milk submitted to manothermosonication. *Journal of Agricultural and Food Chemistry* 50, 6165–6171.
- Vinogradov, I., Khezzer, L., Siginer, D., 2011. Heat transfer of non-Newtonian dilatant power law fluids in square and rectangular cavities. *Journal of Applied Fluid Mechanics* 4 (2), 37–42.
- Wu, J., Gamage, T.V., Vilku, K.S., Simos, L.K., Mawson, R., 2008. Effect of thermosonication on quality improvement of tomato juice. *Innovative Food Science and Emerging Technologies* 9, 186–195.
- Xu, Z., Keijia, Y., Shinobu, K., 2013. Numerical simulation of liquid velocity distribution in a sonochemical reactor. *Ultrasonics Sonochemistry* 20(1), 452–459.
- Zuo, J.Y., Knoerzer, K., Mawson, R., Kemtish, S., Ashokkumar, M., 2009. The pasting properties of sonicated waxy rice starch suspensions. *Ultrasound Sonochemistry* 16, 462–468.